Signatures of criticality in turning avalanches of schooling fish

Andreu Puy [1,*] Elisabet Gimeno [1,2] David March-Pons [1,2] M. Carmen Miguel [2,3] and Romualdo Pastor-Satorras [1]

[1]*Departament de Física, Universitat Politècnica de Catalunya, Campus Nord B4, 08034 Barcelona, Spain*
[2]*Departament de Física de la Matèria Condensada, Universitat de Barcelona, Martí i Franquès 1, 08028 Barcelona, Spain*
[3]*Institute of Complex System (UBICS), Universitat de Barcelona, 08028 Barcelona, Spain*

Moving animal groups transmit information through propagating waves or behavioral cascades, exhibiting characteristics akin to systems near a critical point from statistical physics. Using data from freely swimming schooling fish in an experimental tank, we investigate spontaneous behavioral cascades involving turning avalanches, where large directional shifts propagate across the group. We analyze several avalanche metrics and provide a detailed picture of the dynamics associated with turning avalanches, employing tools from avalanche behavior in condensed-matter physics and seismology. Our results identify power-law distributions and robust scale-free behavior through data collapses and scaling relationships, confirming a necessary condition for criticality in fish schools. We explore the biological function of turning avalanches and link them to collective decision-making processes in selecting a new movement direction for the school. We report relevant boundary effects arising from interactions with the tank walls and influential roles of boundary individuals. Finally, spatial and temporal correlations in avalanches are explored using the concept of aftershocks from seismology, revealing clustering of avalanche events below a designated timescale and an Omori law with a faster decay rate than observed in earthquakes.

I. INTRODUCTION

A fascinating and controversial hypothesis in biology is that some systems may operate close to a critical point from statistical physics, separating an ordered state of the system from a disordered one [1–3]. Biological systems at a critical point are believed to possess functional advantages such as optimality in signal detection, storing, and processing; large correlations in coordinated behavior; and a wide spectrum of possible responses [4–6]. Criticality is often associated with scale invariance, exemplified by power-law distributions lacking relevant characteristic scales besides natural cutoffs [1,2,7]. In particular, this is observed for systems exhibiting spatiotemporal activity in the form of cascades or avalanches with variable duration and size, which at the critical point are distributed as power laws with anomalously large variance. There has been evidence of criticality signatures in many different biological systems, including neural activity and brain networks, gene regulatory networks, collective behavior of cells, or collective motion [4,5,8].

The field of collective motion, in particular, studies the group movement patterns exhibited by social organisms, such as flocks of birds, fish schools, insect swarms, herds of mammals, and human crowds [9,10]. In this context, analytical and experimental studies of moving animal groups suggest the existence of phase transitions between phases of coherent and incoherent motion [11–14]. Moreover, groups of animals can transmit information across the group in the form of propagating waves or avalanches of behavior, as occurs in fish schools [15–20], honeybees [21], bird flocks [22–24], sheep herds [25], or macaque monkeys [26]. Models of collective motion have also reproduced features of these phenomena [27–30]. These behavioral cascades are typically represented by behavioral shifts in the speed, acceleration, or heading of individuals and can arise either spontaneously or from responses to environmental cues, such as the presence of predators, food sources, or obstacles. From a biological point of view, they can occur when individuals follow the behavior of others without regarding their own information [31]. From a physical perspective, behavioral cascades can show signatures typical from systems located near a critical point. Mainly, these signatures include large susceptibility or sensitivity to perturbations [20,26,30,32,33], scale-free correlations [33,34], and possible indications of power-law behavior in the avalanche size distribution [16,19,20,25]. In addition, there is some evidence that the state of criticality can be regulated by moving animal groups depending on their needs [26,30,35], where the avalanche dynamics may transition from being supercritical with local changes propagating through the entire group to critical with changes propagating at all possible scales of the system or to subcritical with changes remaining local [36].

In this study we focus on analyzing the properties of turning avalanches in freely moving fish [19]. These

---

*Contact author: andreu.puy@upc.edu

behavioral cascades involve the propagation of large changes in the heading direction of individuals within a group, often resulting in a reorientation of the group's global trajectory. Specifically, we examine spontaneous turning avalanches of schooling fish freely swimming in a tank. Our investigation unveils scale-free properties in the statistical distributions of different avalanche metrics and their dependence on the number of individuals in the school. Additionally, we investigate the origins of these avalanches, analyzing their triggering with respect to space, time, and individual initiators. Our findings reveal the relevance of interactions with tank walls and a larger influence of boundary individuals. We also explore the dynamical evolution of avalanches and its relation with the state of the school, as well as their spatial and temporal correlations. Within the limits of our experimental setup, our results strongly suggest the presence of a scale-free avalanche dynamics, which could be compatible with the school operating in the vicinity of a critical point.

II. AVALANCHE DEFINITION AND BASIC OBSERVABLES

Behavioral cascades in fish have been defined measuring changes of different quantities. Here we focus on avalanches defined in terms of large changes in the heading of individuals, given by their velocity vector [19]. As an experimental subject, we consider the motion of $N = 8$, 16, 32, and 50 individuals of the species of black neon tetra *Hyphessobrycon herbertaxelrodi*, a social fish that tends to form polarized, compact, and planar schools, freely swimming in an approximately two-dimensional experimental tank. We recorded and digitized individual fish trajectories and calculated the corresponding velocities and accelerations (refer to Appendix A for experimental and data acquisition details). In order to remove the dependence on the experimental frame rate of the recordings, we measure the changes in time of the heading in terms of the turning rate ω, defined as the absolute value of the angular velocity, i.e.,

$$\omega = \frac{|\vec{v} \times \vec{a}|}{v^2},\tag{1}$$

where $\vec{v}$ and $\vec{a}$ are the instantaneous velocity and acceleration of an individual, respectively, and v is the modulus of the instantaneous velocity. (See Appendix B for a derivation of this expression.) We consider the absolute value due to symmetry in the turning direction.

In Fig. 1(a) we show the probability density function (PDF) of the turning rate $P(\omega)$ for schools of different numbers of individuals N. Here and in the following, we work in natural units of pixels and frames for distance and time, respectively. In addition, error bands in the PDF plots are calculated from the standard deviation of a Bernoulli distribution with the probability given by the fraction of counts in each bin of the numerical PDF [37]. As we can see, schools of different numbers of individuals show essentially the same behavior in their turning rate distributions. Most of the time, the turning rate is very small and uniformly distributed, corresponding to fish swimming locally in a straight trajectory. In some instances, however, large turning rates can be observed, in which individuals swiftly rearrange their headings and thus reorient their direction of motion.
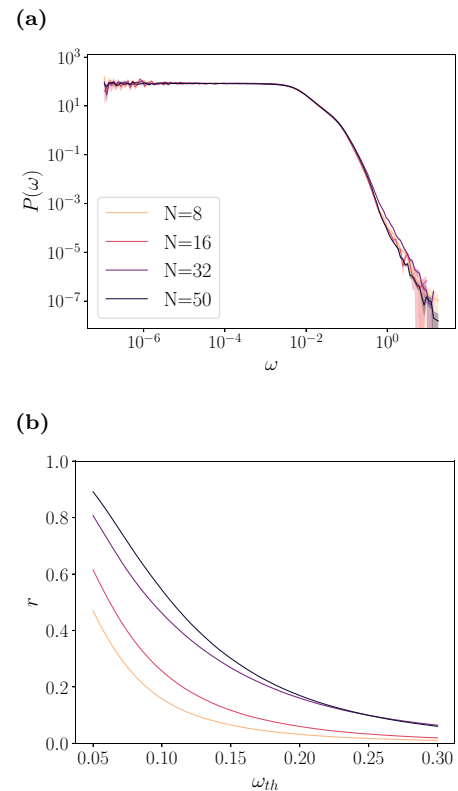

FIG. 1. (a) PDF of the turning rate ω and (b) activity rate r of turning avalanches as a function of the turning threshold ω_{th}. The different curves correspond to experimental data from schools with different numbers of individuals N. Quantities are expressed in natural units of frames and pixels.

Inspired by avalanche behavior in condensed-matter physics [38], we define avalanches by introducing a turning threshold ω_{th} separating small turns from large ones [19]. Considering an active fish as one with a turning rate $\omega > \omega_{th}$, we introduce the dynamical variable n_t defined as the number of active fish observed at frame t. Then sequences of consecutive frames in which $n_t > 0$ (i.e., in which there is at least one active fish) define a turning avalanche. In video S1 of the Supplemental Material [39] we show some examples of large turning avalanches for a school of $N = 50$ fish.

The most basic characterization of turning avalanches is given by the duration T and size S of avalanches and by their interevent time t_i. An avalanche starting at frame t_0 has duration T if the sequence of dynamic variables n_t fulfills $n_{t_0-1} = 0$, $n_t > 0$ for $t = t_0, \ldots, t_0 + T - 1$, and $n_{t_0+T} = 0$. The size S of an avalanche is given by the total number of active fish in the whole duration of the avalanche, i.e., $S = \sum_{t=t_0}^{t_0+T-1} n_t$. The interevent time t_i between two consecutive avalanches is given by the number of frames between the end of one avalanche and the start of the next one, that is, by a sequence fulfilling $n_{t_f} > 0$, $n_t = 0$ for $t = t_f + 1, \ldots, t_f + t_i$, and $n_{t_f+t_i+1} > 0$, where t_f indicates the last frame of the first avalanche [40].

The effects of the turning threshold in avalanches can be assessed with the activity rate r, defined as the probability that a randomly chosen frame belongs to an avalanche. We
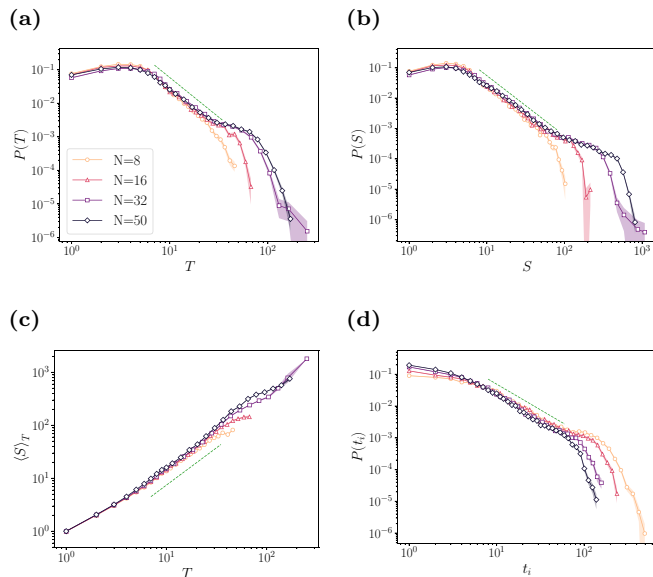
FIG. 2. (a) PDF of the duration T, (b) PDF of the size S, (c) average size $\langle S \rangle_T$ as a function of the duration T, and (d) PDF of the interevent time t_i for $\omega_{\text{th}} = 0.1$. The different curves correspond to schools of different numbers of individuals N. The exponents from the green dashed power laws are (a) $\alpha = 2.4 \pm 0.2$, (b) $\tau = 1.97 \pm 0.14$, (c) $m = 1.41 \pm 0.06$, and (d) $\gamma = 1.62 \pm 0.08$.

compute it as the ratio between the number of frames with activity $n_t > 0$ and the total number of frames in the experimental series. As we can see from Fig. 1(b), for fixed N the activity rate decreases with the turning threshold ω_{th}, since by increasing ω_{th} we are decreasing the turning rates that we consider large and we find fewer frames with $n_t > 0$. On the other hand, increasing the number of individuals N at fixed ω_{th} results in an increase of the activity rate. We can interpret this as a school with a larger number of individuals has a higher probability for any of them to display a large turning rate.

Realistic values of ω_{th} used to compute avalanches are estimated to lie within the range $\omega_{\text{th}} \in [0.01, 0.3]$. Smaller values result in infinite avalanches that span the entire duration of the experiment, whereas larger values produce very few avalanches.

III. STATISTICAL DISTRIBUTIONS

In Figs. 2(a) and 2(b) we show the distributions of the duration T and size S, respectively, obtained for a fixed turning threshold $\omega_{\text{th}} = 0.1$ and for schools of different numbers of individuals N. We find that both PDFs show a power-law scaling region of the form

$$P(T) \sim T^{-\alpha}, \quad P(S) \sim S^{-\tau}, \tag{2}$$

limited by a peak for low values and a shoulder or bump with a fast decaying (exponential) tail for high values. The characteristic exponents α and τ, obtained from a linear regression in double-logarithmic scale in the scaling region, take the values $\alpha = 2.4 \pm 0.2$ and $\tau = 1.97 \pm 0.14$, where the error bars represent 95% confidence intervals. Different values of ω_{th} lead to similar average exponents, e.g., $\alpha = 2.9 \pm 0.8$ and $\tau = 2.4 \pm 0.4$ for $\omega_{\text{th}} = 0.15$ (see Fig. S1 in the Supplemental

Material [39]). These exponents align with previous estimates derived from smaller statistics and using a different definition of turning fish [19]. Interestingly, distributions for schools of different numbers of individuals collapse onto the same functional form with the exception of the tail, which can be interpreted in terms of finite-size effects, as larger schools tend to create avalanches of larger duration and size.

The duration and size of individual avalanches are not independent, as we can check by plotting the average size $\langle S \rangle_T$ of avalanches of duration T [see Fig. 2(c)]. From this figure we can observe a superlinear behavior

$$\langle S \rangle_T \sim T^m, \tag{3}$$

with $m = 1.41 \pm 0.06$. The value of m can be related to the exponents of the duration and size distributions as [19,36]

$$m = \frac{\alpha - 1}{\tau - 1}.$$

Our experimental value m is fully compatible with the theoretical prediction $m = 1.4 \pm 0.3$ for $\omega_{\text{th}} = 0.1$ [experimental $m = 1.35 \pm 0.16$ and theoretical prediction $m = 1.4 \pm 0.7$ for $\omega_{\text{th}} = 0.15$ (see Fig. S1c in [39])].

In Fig. 2(d) we show the PDF of the interevent time t_i for $\omega_{\text{th}} = 0.1$ and for schools of different numbers of individuals N. We find again an intermediate scale-free region, limited between the small-time behavior and a shoulder with an exponentially decreasing tail. Here also plots for different numbers of individuals N collapse on the same functional form, with the exception of the tail. A fit to the form

$$P(t_i) \sim t_i^{-\gamma}$$

in the scaling region leads to an average exponent $\gamma = 1.62 \pm 0.08$ [$\gamma = 1.63 \pm 0.04$ for $\omega_{th} = 0.15$ (see Fig. S1d in [39])]. It is noteworthy that the behavior of the decaying tails with N is reversed with respect to the duration and size PDFs, with a larger number of individuals leading to smaller interevent times. This observation is consistent with the behavior of the activity rate r, as schools with a larger number of individuals have a higher probability to be in an avalanche.

IV. DATA COLLAPSE

The dependence of the tails on the duration and size distributions with the school size N observed above and with the turning threshold ω_{th} reported in [19] suggests the possibility of a relationship between ω_{th} and N resulting in avalanches with collapsing distributions. In order to test for this hypothesis, we select the threshold ω_{th} that, for each value of N, leads to a fixed activity rate $r = r_0$. From Fig. 1(b) we estimate, for $r_0 = 0.4$, $\omega_{\text{th}} = 0.055, 0.076, 0.11, 0.13$ for $N = 8, 16, 32, 50$, respectively. We plot the resulting distributions in Figs. 3(a), 3(b), and 3(c) for the duration T, size S, and interevent time t_i, respectively. In a system with no temporal correlations in the activity of individuals, a fixed activity rate results in duration and interevent time distributions collapsing onto the same functional exponential forms (see Appendix C). Surprisingly, even if this is not the case for empirical turning avalanches in schooling fish, both the duration and interevent time distributions achieve a data collapse at fixed r. On the other hand, the size distributions do not collapse perfectly,
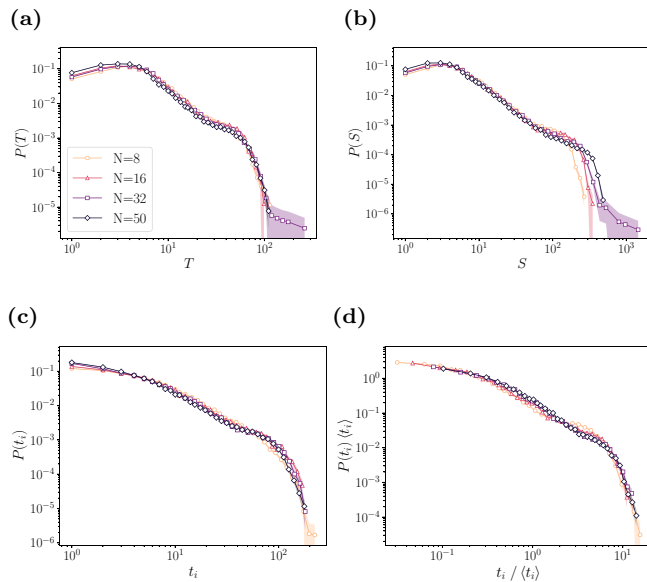
FIG. 3. Data collapse for the PDFs of (a) the duration T, (b) the size S, and (c) the interevent time t_i for schools of different numbers of individuals N considering avalanches with a fixed activity rate $r = 0.4$ (corresponding to $\omega_{\text{th}} = 0.055, 0.076, 0.11, 0.13$ for $N = 8, 16, 32, 50$, respectively). (d) Data collapse of the interevent time given by Eq. (4) for $\omega_{\text{th}} = 0.1$.

possibly because of correlations in the turning rates of individuals at a given frame, which results in more active individuals in an avalanche frame for schools of larger numbers of individuals. Interestingly, also in the uncorrelated case, the size distributions are not expected to collapse (see Appendix C).

On a similar note, for avalanches of self-organized critical phenomena across different contexts, it has been found that the interevent time distributions can be collapsed into the scaling form [41,42]

$$P(t_i) = \frac{1}{\langle t_i \rangle} \Phi\left(\frac{t_i}{\langle t_i \rangle} \right), \qquad (4)$$

where $\Phi(x)$ is a universal scaling function and the only characteristic scale is the average interevent time $\langle t_i \rangle$. In Fig. 3(d) we show this sort of collapse for a turning threshold $\omega_{th} = 0.1$; as we can see, it also applies to turning avalanches in schooling fish. This reveals self-similar behavior, with the interevent time distributions only differing in their average value for schools of different numbers of individuals. In the uncorrelated case, this collapse is also recovered, but now only in the limit of a large average interevent time (see Appendix C).

As a final check of the scale-free nature of turning avalanches, we consider the scaling of the avalanche shape n_t, defined by the number of active individuals of a turning avalanche at the frame t of its duration [43]. Many scale-free avalanche systems exhibit a collapse behavior in the avalanche shape given by the scaling relation

$$n_t = T^{m-1} \Phi(t/T),$$

where $m = (\alpha - 1)/(\tau - 1)$ is the exponent relating the average avalanche size $\langle S \rangle_T$ with the duration T [Eq. (3)] and $\Phi(z)$
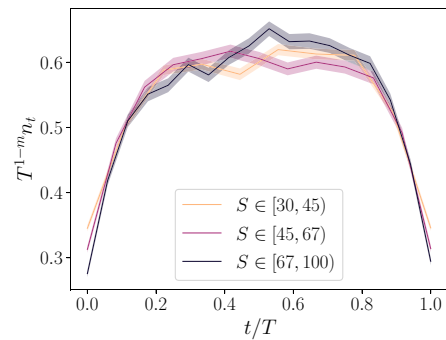

FIG. 4. Rescaled avalanche shape $T^{1-m} n_t$ as a function of the normalized time t/T. Avalanche shapes are averaged over similar sizes S within the power-law scaling region of the size distribution.

is a universal scaling function [6,43–45]. In the case of turning avalanches, this scaling behavior is recovered in avalanches within the power-law scaling regime of the size distribution, as shown in Fig. 4. In this plot the avalanche shape is computed by normalizing the avalanche time frame t by its duration T and averaging over avalanches in a given size range. We use the value $m = 1.41$ obtained in the numerical analysis of the duration and size distributions.

V. AVALANCHE TRIGGERING

In this section we explore whether avalanches are triggered in some preferential points in space or time, as well as by particular individuals in the group. Here and in the following sections we show results for avalanches in a school of $N = 50$ individuals, which have the longest recording time, and a turning threshold $\omega_{\text{th}} = 0.1$.

A plausible hypothesis is that avalanches are more frequently triggered near the tank walls due to boundary effects. These could arise when fish are approaching a wall and need to perform a large turn in order to avoid colliding with it. To check this hypothesis we consider the position for the center of mass (cm) $\vec{x}_{\text{c.m.}}$ of the school, defined as

$$\vec{x}_{\text{c.m.}} \equiv \frac{1}{N} \sum_i \vec{x}_i,$$

where $\vec{x}_i$ are the positions of the fish at a given instant of time. We define the triggering location of an avalanche as the position of the c.m. at the first frame t_0 of the avalanche. We study the distribution of triggering locations on the surface of the tank. Because fish do not swim uniformly all around the tank, in order to extract a statistically significant density of triggering locations, we normalize their counts against the counts of all observed positions of the cm along the time evolution of the school. We show this in Fig. 5(a), where the axis orientations correspond to the tank walls. The gray region in the colormap, separating the low-density (red) and high-density (blue) values, corresponds to the expected density in the absence of correlations, which we calculate from the total counts of triggering locations divided by the total counts of positions of the cm As we can see in this plot, the distribution of avalanches in the tank is quite homogeneous, although there is a slight tendency for avalanches to occur
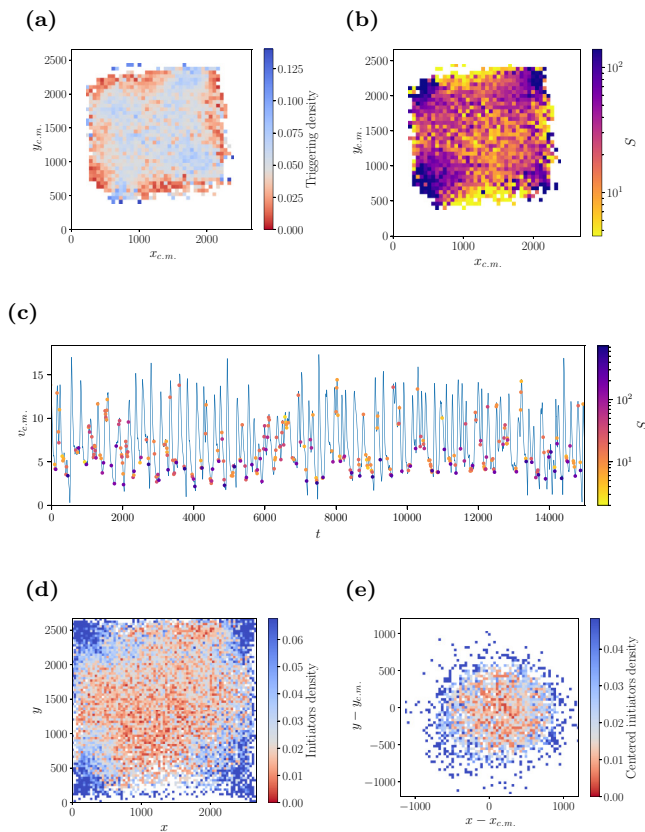
FIG. 5. Avalanche triggering in space, in time, and within the group. (a) Density for the position of the center of mass $\vec{x}_{cm}$ at the start t_0 of an avalanche (the triggering location) normalized against all trajectories of the center of mass, (b) average size S for triggering locations of avalanches, (c) blue line showing the temporal evolution for the center of mass speed v_{cm} and dots showing avalanches triggered at the given speed v_{cm} and time t_0 and colored by their size S, (d) and (e) density for the position of initiators normalized against the positions of all individuals at the start t_0 of an avalanche for (d) the laboratory reference frame and (e) the center-of-mass reference frame and only for centered individuals. In (a), (d), and (e) the gray color in the colormap corresponds to the expected density in the absence of correlations, given by the total counts of the quantity considered divided by the total counts of the normalization. In (c) we only plot avalanches that propagated to individuals other than the ones active in the first frame of the avalanche. In (e) the y coordinate is oriented in the direction of motion of the group given by the center-of-mass velocity.

away from the walls. However, if we display the average size S of avalanches generated at the different triggering locations, we obtain a different picture [Fig. 5(b)], in which avalanches of larger sizes tend to occur more frequently near the tank corners. This observation suggests that interactions with the tank walls indeed promote the emergence of large turning avalanches, resulting in important orientation rearrangements of the school.

Since large avalanches seem to be originating from interactions with the walls, we investigate whether these interactions are responsible for the shoulder or bump observed in the the tails of the duration and size distributions. They are particularly noticeable in groups with larger numbers of

individuals ($N = 32$ and 50), which are expected to have more frequent interactions with the tank walls. This feature, known as dragon kings, breaks the power-law paradigm by displaying overrepresented extreme events [46–48]. Dragon kings are typically generated by mechanisms different from those of smaller events, which, in this case, may be wall interactions. To explore this, we analyze the statistical distributions of avalanches with triggering locations away from the walls, which we restrict to occur inside the square positioned at the center of the tank with side $L/3$, where L is the side of the tank (refer to Fig. S2 in [39]). We expect these avalanches to arise spontaneously and not be promoted by interactions with the tank walls. Despite limited statistics, dragon kings are no longer observed, and the distributions now showcase extended power-law regions with the same characteristic exponents as previously measured. We quantify the presence of dragon kings in the size distribution for $N = 50$ with a statistical dragon king detection test [48,49] (see Appendix D). Employing a significance level $\alpha = 0.05$ for the null hypothesis that there are no dragon kings, the test confirms dragon kings (p value $p < 10^{-15}$) for the total size distribution [Fig. 2(b)] and rejects their presence ($p = 0.1$) for the size distribution restricted to the central region of the tank (Fig. S2 in [39]).

To understand temporal triggering of avalanches, we study how the avalanche starting time t_0 relates to the group dynamics represented by the center-of-mass speed $v_{c.m.}$, which is defined as

$$v_{c.m.} \equiv \left| \frac{1}{N} \sum_i \vec{v}_i \right|. \tag{5}$$

The center-of-mass speed is characterized by having oscillations due to a burst-and-coast mechanism of the individuals [50–52], with increases associated with an active phase powered by the fish muscles and decreases coming from a passive gliding phase. In Fig. 5(c) we plot, for a time window of 5 min from a single recording, the temporal evolution of the center-of-mass speed as the blue line. We mark with dots avalanches triggered at the corresponding time t_0 and speed $v_{c.m.}$, color coded by their size S. We only consider avalanches that propagated to individuals other than the ones active in the first frame of the avalanche. As we can observe, while small-size avalanches tend to be randomly distributed over different values of $v_{c.m.}$, large avalanches are more often located near the minima of the speed, even when the minimum changes across time. We notice that this behavior does not originate from small speeds being related to large turning rates, because we find the turning rate is inversely related to the speed only for $v_{cm} < 4$ and appears to be independent for larger speeds (see Fig. S3 in [39]). Instead, this suggests that large avalanches may emerge from turnings related to decision-making processes occurring at the onset of the active phase of the burst-and-coast mechanism [51,53,54].

Apart from the spatiotemporal triggering of avalanches, we can study how avalanches are triggered at the individual level within the school considering avalanche initiators, defined as the individuals that are active in the first frame of the avalanche. Previously, it was observed that some individuals have a probability larger than random fluctuations to be the initiators of behavioral cascades [19]. Here instead we focus
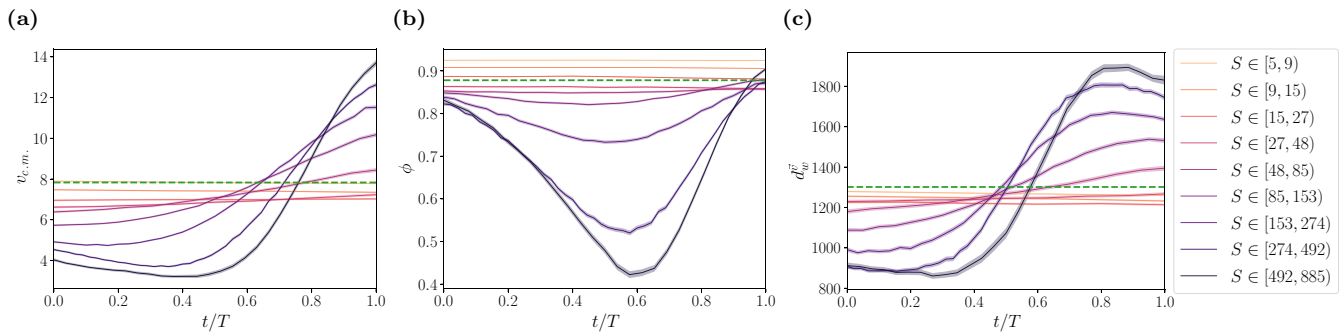
(a)

(b)

(c)

FIG. 6. Dynamics within turning avalanches of (a) the center-of-mass speed v_{cm}, (b) the polarization ϕ, and (c) the directed wall distance $d_w^{\vec{v}}$ depending on the normalized time t/T and averaged for similar sizes S. The green dashed horizontal line is the average of the given variable over the whole experiment.

on the location of individual initiators within the experimental tank and inside the school. Again, we have to keep in mind that individuals are not located uniformly around the tank at the start of an avalanche. Therefore, in order to extract a statistically significant density of initiator locations within the group, we normalize their counts against the counts of the positions of all individuals at the onset time t_0 of the avalanche. We show the resulting plot in Fig. 5(d). We find that initiators tend to accumulate near the tank walls and particularly at the corners. This is compatible with the idea that large turning avalanches are promoted by interactions with the tank walls.

In order to explore the natural relative position of avalanche initiators within the school, we select individuals that do not have relevant interactions with the tank walls. We define centered individuals as those that are positioned in the central square of the tank with side $L/3$, where L is the side of the tank. If we plot the density of the positions of centered initiators within the tank normalized by the positions of all centered individuals at the onset time t_0 of an avalanche (see Fig. S4 in [39]), indeed we see a uniform pattern that confirms the idea that centered initiators do not experience significant interactions with the tank walls. We study the relative position of centered initiators within the school in Fig. 5(e), where we plot the density of the positions of centered initiators normalized against all centered individuals at the triggering time t_0 of the avalanche in the center-of-mass reference frame. In this plot the y coordinate is directed in the direction of motion of the center of mass. As we can see, initiators of avalanches away from the tank walls accumulate on the boundary of the school and without any preferred direction along the movement of the group.

VI. DYNAMICAL EVOLUTION OF AVALANCHES

In this section we examine how an avalanche can affect the behavior of the whole group by measuring several group properties along the evolution of the avalanche. In order to compare avalanches with different sizes S, as in the case of the avalanche shape discussed above, we first normalize the temporal evolution of the avalanche by its duration T and then average the dynamics over groups of avalanches with similar sizes.

First, we investigate the speed of the group given by the center-of-mass speed v_{cm}, defined in Eq. (5). We show how

it evolves during a turning avalanche, averaged for different sizes S, in Fig. 6(a). For comparison, we plot the average value over the whole experiment as the green dashed horizontal line. We observe that avalanches tend to start below the average v_{cm} and that avalanches of small size do not alter the school speed noticeably. On the other hand, larger-size avalanches tend to originate at lower values of v_{cm} and increase the school speed during their evolution.

As a second characteristic of the school we consider the global order measured in terms of the polarization ϕ [12],

$$\phi \equiv \left| \frac{1}{N} \sum_i \frac{\vec{v}_i}{v_i} \right|,$$

which tends to 1 if the school is ordered and all individuals move in the same direction and takes a value close to zero if the school is disordered and fish move in random and independent directions [12]. We show its evolution within an avalanche in Fig. 6(b). Small-size avalanches tend to start in highly polarized configurations and do not change significantly the level of order. Contrarily, large avalanches tend to start with less-ordered configurations than the average and further reduce the order as the avalanche spreads. However, at later stages this trend is reversed and the school recovers a highly ordered state.

To gain further information about the possible role of the walls, we study the dynamical evolution of avalanches with respect to the distance to the tank walls. We define the directed wall distance $d_w^{\vec{v}}$ as the distance from the center of mass of the school to the tank walls in the direction of the velocity of the center of mass. For a square tank, this distance is defined as

$$d_w^{\vec{v}} \equiv \min\left[\sqrt{1 + \left(\frac{v_y}{v_x}\right)^2} [\Theta(v_x)(L-x) + \Theta(-v_x)x], \right.$$

$$\left. \times \sqrt{1 + \left(\frac{v_x}{v_y}\right)^2} [\Theta(v_y)(L-y) + \Theta(-v_y)y] \right],$$

where the positions $\vec{x}$ and velocities $\vec{v}$ refer to the center of mass; $\Theta(x)$ is the Heaviside step function, which discriminates the forward and backward motion; L is the side of the tank; and the two terms in the min function refer to the walls on the x and y coordinates, respectively. We plot the evolution of this quantity during turning avalanches in Fig. 6(c). As we

can observe, small-size avalanches do not alter the directed wall distance. On the other hand, large avalanches tend to start closer to the wall and end at higher directed distances. This indicates that large turning avalanches typically produce a large change of the group orientation from facing a nearby wall to facing a farther away wall. We have also studied the evolution of the distance to the nearest wall, which we refer as the minimum wall distance d_w,

$$d_w \equiv \min(x, L - x, y, L - y).$$

We observe (see Fig. S5 in [39]) that this quantity decreases and has a minimum for large avalanche sizes, indicating that during the avalanche evolution the school tends to approach the closest wall, to later move away from it.

VII. AVALANCHE CORRELATIONS

Another important aspect in avalanche behavior is the presence of correlations, namely, whether the occurrence of an avalanche induces the occurrence of other avalanches such that they appear clustered in space and/or time [42]. The idea of correlations and clustering in avalanches is closely linked to the concept of main events and aftershocks in seismology [55]. In this context, aftershocks are typically smaller events that occur after a main event in nearby locations and stand out from the background noise. A relevant result here is the observation of the Omori law, which states that the probability to observe an aftershock at a given time t after a main event follows the distribution

$$P(t) = \frac{K}{(t + c)^p}, \qquad (6)$$

where K, c, and p are constants, with $p \sim 1$ [56].

In seismology, earthquakes are quantified by their magnitude, which is a measure related to the logarithm of the energy released. Analogously, for turning avalanches we can introduce the magnitude m as

$$m \equiv \ln S,$$

where S is the size of the avalanche. Considering the observed size distribution from Eq. (2), magnitudes for turning avalanches follow the distribution

$$P(m) \sim e^{-bm}, \qquad (7)$$

with $b = \tau - 1$, which is analogous to the well-known Gutenberg-Richter law for earthquakes [57].

In order to classify events (either earthquakes or avalanches) into main events and aftershocks, we consider the method proposed by Baiesi and Paczuski [58,59]. This method is based on the definition of the proximity η_{ij} in the space-time-magnitude domain from an event j to a previous (in time) event i [58,60,61]. Assuming that events are ordered in time $t_1 < t_2 < t_3 < \cdots$, the proximity is defined as

$$\eta_{ij} \equiv \begin{cases} t_{ij} r_{ij}^d P(m_i) & \text{if } i < j \\ \infty & \text{otherwise,} \end{cases}$$

where t_{ij} is the time interval between events i and j, r_{ij} is the spatial distance between the events locations, d is the fractal dimension of the set of events positions, and $P(m_i)$ is
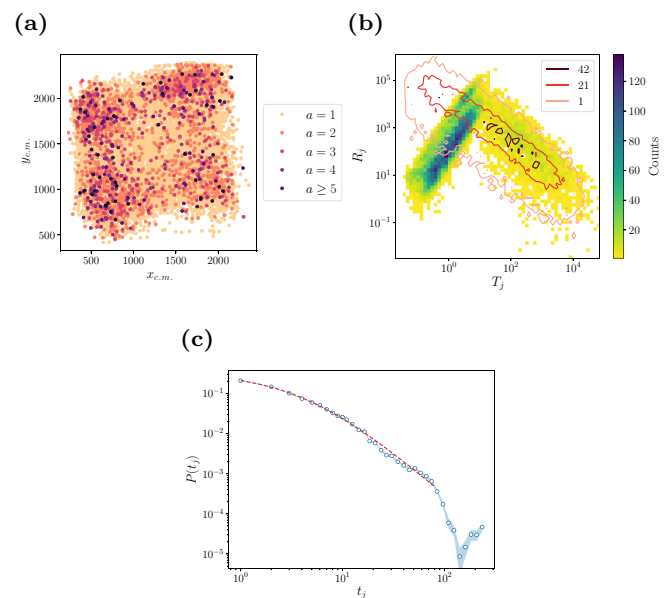

FIG. 7. Correlation measures of aftershocks: (a) number of aftershocks a per parent depending on the triggering location of the parent, (b) counts for the joint distribution of the rescaled space R_j and time T_j (the contour plot corresponds to randomized avalanches, in which avalanche positions, interevent times, and magnitudes have been shuffled), and (c) PDF for the time interval t_j between parents and aftershocks for $t_j < 250$. We only considered avalanches with magnitudes $m \geqslant 1.6$. In (c) the red dashed line corresponds to a fit to the Omori law (6) with $c = 4.3 \pm 0.4$ and $p = 2.2 \pm 0.1$.

the Gutenberg-Richter law for event i, which in our case is given by Eq. (7). In the context of turning avalanches, we have to consider two facts. (i) Avalanches have a finite duration that is comparable to the interevent time between consecutive avalanches. We therefore consider t_{ij}, $i < j$, as the number of frames between the end of avalanche i and the start of avalanche j. (ii) During an avalanche, the school moves. We thus consider the distance r_{ij}, $i < j$, as the distance between the center of mass of the school at the end of avalanche i and the center of mass of the school at the beginning of avalanche j. Additionally, the distribution of the positions of the center of mass at the start of avalanches does not seem to show a fractal structure, so we use here $d = 2$.

The proximity η_{ij} is a measure of the expected number of events of magnitude m_i to occur, looking backward in time from event j within a time interval t_{ij} and distance r_{ij}, in the absence of correlations, in such a way that the time and position of previous avalanches behave as independent Poisson processes [58]. Therefore, smaller values of the proximity are associated with a larger probability that the events i and j are actually correlated.

Using the proximity η_{ij}, every event j can be associated with a nearest neighbor or parent p_j, defined as the event in the past ($p_j < j$) that minimizes the proximity with j, namely, $\eta_{p_jj} \leqslant \eta_{ij} \forall i < j$. This proximity is referred to as the nearest-neighbor proximity η_j, its time interval t_j, and the spatial distance r_j. The set of events with the same parent is considered the aftershocks of that parent. In Fig. 7(a) we examine the distribution of the triggering locations of parents,

color coded by their number of aftershocks a. We find a possible influence of the tank walls, as parents with a larger number of aftershocks tend to be located closer to the corners.

In addition, we consider the measure of clustering proposed within this framework in Ref. [60]. This formalism is based in the rescaled time T_j and rescaled space R_j [60,61], defined as

$$T_j \equiv t_j \sqrt{P(m_{p_j})},$$

$$R_j \equiv (r_j)^d \sqrt{P(m_{p_j})}$$

such that

$$\eta_j = T_j R_j.$$

In real earthquakes, it is observed that the joint distribution of T_j and R_j is bimodal. One mode corresponds to background events and is compatible with a random (Poisson) distribution of times and positions of events. The other mode, on the other hand, corresponds to clustered events, correlated in space and time [61].

In Fig. 7(b) we show the joint distribution of T_j and R_j for turning avalanches in terms of a color density plot. In the same figure, we display in terms of a contour plot the joint distribution obtained for randomized data, in which avalanche positions, interevent times, and magnitudes have been shuffled. We find that the experimental data show clearly two modes in the distribution. In one mode, for large values of T_j, increasing the rescaled time T_j results in a decrease of the rescaled space R_j. This is almost identical to the distribution obtained for the shuffled data, indicating that it corresponds essentially to background, uncorrelated noise. The other mode occurs for smaller values of T_j and displays the opposite behavior, increasing the rescaled time T_j results in a higher rescaled space R_j. This behavior is different from the background noise and corresponds to clustered (correlated) avalanches.

We can understand the timescale separation between the modes taking into account that turning avalanches take place inside a school that is moving around the tank. The school typically performs a recurrent movement on the tank, visiting a given point in the tank with some average period. We can quantitatively analyze this behavior looking at the mean-square displacement of the position of the center of mass, which measures the average displaced distance of the group in time starting from any point in the trajectory (see Fig. S6 in [39]). The first maximum occurs around $t_c = 250$ frames and corresponds to the average time the school needs to perform a half-turn around the tank and becomes maximally separated from its initial position. Aftershocks with a lower time interval tend to increase their spatial distance as the school moves away from the parent location. After this time and up to very large time intervals, the school may return towards the parent position and we can find aftershocks occurring at lower spatial distances. However, these tend to occur rather randomly and cannot be distinguished from random events. This highlights a major difference with earthquakes, where significant correlations can occur in the same location at widely separated time intervals.

Finally, we examine the Omori law displaying the distribution for the time interval t_j between parents and aftershocks in Fig. 7(c). The distribution is computed considering the sequences of aftershocks for each parent, shifting the sequences to set each parent at a common time zero, and stacking all sequences in a single common sequence [62]. From the above reasons, we only consider time intervals below $t_c = 250$ that correspond to significant correlated aftershocks. A least-squares fitting of the empirical data to the Omori law given by Eq. (6) (green dashed line) yields the parameters $c = 4.3 \pm 0.4$ and $p = 2.2 \pm 0.1$. This indicates a value $p > 1$, implying a faster decay rate of aftershocks than in earthquakes.

VIII. CONCLUSION

In this paper we have presented an empirical analysis of spontaneous behavioral cascades in schooling fish considering turning avalanches, where large turns in the direction of motion of individuals are propagated across the group. This was achieved by collecting extensive state-of-the-art tracking data for schooling fish, comprising up to 1.8×10^5 time samplings at a resolution of 50 frames/s, for experiments involving varying numbers of fish, up to groups of 50 individuals. This data set yielded over 10^4 avalanche events, representing a significant advancement compared to previous studies on behavioral cascades (for reference, in [30] the authors reported 10^2 avalanche events). We have analyzed different avalanche metrics and provided a highly detailed picture of the dynamics associated with behavioral cascades, employing tools from avalanche behavior in condensed-matter physics and seismology.

We have uncovered evidence of scale-free behavior across various aspects of turning avalanches in schooling fish. Analysis of probability distributions for fundamental observables, such as the avalanche duration, size, and interevent times, revealed long tails compatible with power-law forms. Adjusting for dragon king events, which are disproportionately represented by extreme events induced by interactions with tank walls, we found the power-law region for avalanche size extended up to two decades. We also established a scaling relationship between the characteristic exponents of the duration and size distributions. Furthermore, a data collapse in the distributions of the duration and interevent times at a fixed activity rate indicates a connection in avalanche dynamics across schools with varying numbers of individuals and the turning threshold defining the avalanche. We also confirmed two previously observed data collapses in critical avalanche systems: in the interevent times distribution normalized by the mean and in the avalanche shape or mean temporal profile via a scaling relationship with the duration.

While power laws are often attributed to critical phenomena related to phase transitions, alternative mechanisms can also produce such distributions [4,63]. A tighter prediction of criticality is manifested through data collapses and relations between scaling exponents [4,44,45], indicating quantitative universal avalanche dynamics across scales. Ultimately, these findings are insufficient to demonstrate criticality, but they constitute necessary conditions and embody a crucial theoretical aspect that has received limited attention in behavioral

cascades of moving animal groups. In our work, we addressed this gap and complemented existing studies, providing evidence that fish schools could operate in the vicinity of a critical point. In particular, given the apparent lack of externally tuned parameters in the system, they would represent an instance of self-organized criticality [8,64]. While our experimental settings are currently limited to studying small group sizes of up to 50 individuals, future work should aim to test for criticality effects in larger groups, involving hundreds or thousands of individuals, to draw adequate comparisons with statistical physics systems.

Being near a critical point can offer advantages such as efficient collective decision-making and information transfer across the group [4,5,8,20]. In this context, turning avalanches may arise from self-organized critical processes that facilitate information exchange among members of a social system, comparable to avalanches seen in the social interactions of collective knowledge creation [65,66]. Specifically, turning avalanches allow fish to decide collectively on their direction of movement. For this reason, it is not surprising that we observe large avalanches occurring at the onset of the active phase of the burst-and-coast mechanism in fish locomotion, where decision-making processes to change individual directions are believed to occur [51,53,54]. During the process of deciding a new collective direction, coordination and group order decrease. However, once a new direction is chosen, speed increases and coordination reemerges. A similar behavior was observed in the phenomenon of collective U-turns, involving directional switches for fish swimming in a ring-shaped tank [18,67]. We argue that collective U-turns can be understood as a specific example of turning avalanches.

Boundary effects, arising from interactions with tank walls or distinct behaviors of individuals at the group's border, are frequently overlooked in the study of animal collective motion. This work highlighted significant effects of tank walls on avalanche behavior. While walls do not increase the number of avalanches, those in their proximity often exhibit larger sizes and manifest in correlated clusters, resulting in a higher occurrence of aftershocks. Moreover, individuals that are initiators of avalanches are more frequently found near walls. This phenomenon can be attributed to the tank walls acting as obstacles, disrupting the group's movement and prompting collective decisions for a subsequent direction away from the walls [68,69]. Notably, large avalanches induced by tank walls primarily impact the tail of duration, size, and interevent time distributions, manifesting as shoulders or dragon kings. The intermediate scale-free behavior in these distributions appears to be intrinsic to spontaneous turning avalanche mechanisms, rather than being promoted by the walls. Additionally, boundary effects from individuals at the group's border play a role, as they are often initiators of avalanches. This aligns with previous findings associating these positions with higher social influence [16,70]. An alternative explanation is that individuals at the group's border may be more exposed to risks [71], maintaining a heightened alert state and making them more prone to initiating a large change of direction.

We have examined the spatial and temporal correlations in turning avalanches through the concept of aftershocks [42].

We observed that turning avalanches of schooling fish reveal significant clustered and correlated events below a time interval corresponding to a half-turn of the school around the tank. This observation points to a fundamental property linked to the absence of collective memory for larger timescales [13]. Furthermore, we found that the probability rate of observing correlated aftershocks after a main event in turning avalanches follows an Omori law with a decay rate exponent $p \sim 2$, significantly faster than in seismology ($p \sim 1$).

We believe this work makes a contribution to the ongoing inquiry into criticality, particularly within the realm of animal collective motion and, more broadly, in biological systems. The limited number of analyses conducted on large data sets with experimental evidence of self-similar behavior, a hallmark of critical systems, highlights the need for further exploration and clarification in this area. Future experiments should aim to study larger systems over longer periods of time to deepen our understanding of these phenomena.

APPENDIX A: EXPERIMENTAL DATA

We employ schooling fish of the species black neon tetra (*Hyphessobrycon herbertaxelrodi*), a small freshwater fish with an average body length of 2.5 cm that has a strong tendency to form cohesive, highly polarized, and planar schools [72]. The experiments, performed at the Scientific and Technological Centers UB, University of Barcelona (Spain), were reviewed and approved by the Ethics Committee of the University of Barcelona (Project No. 119/18). They involved schools of $N = 8$, 16, 32, and 50 individuals freely swimming in a square tank of side $L = 100$ cm with a water column 5 cm deep, resulting in an approximately two-dimensional movement. Videos of the fish movement were recorded with a digital camera at 50 frames/s, with a resolution of 5312×2988 pixels per frame, the side of the tank measuring $L = 2730$ pixels. Digitized individual trajectories were obtained from the video recordings using the open source software idtracker.ai [73]. Invalid values returned by the program caused by occlusions were corrected in a supervised way, semiautomatically interpolating with spline functions (now incorporated in the Validator tool from version 5 of idtracker.ai). For better accuracy, we projected the trajectories in the plane of the fish movement, warping the tank walls of the image into a proper square (for details see Ref. [74]). We smoothed the trajectories with a Gaussian filter [75] with $\sigma = 2$ and truncating the filter at 5σ, employing the `scipy.ndimage.gaussian_filter1d` function from the SCIPY PYTHON scientific library [76]. Individual ve-

locities and accelerations were obtained from the Gaussian filter using first and second derivatives of the Gaussian kernel, respectively.

We discarded recordings where fish stop for prolonged periods. We implement this quantitatively by applying a Gaussian filter with $\sigma = 200$ to the mean speed of individuals $\langle v \rangle$ and discarding sequences that go below a given threshold $\langle v \rangle_{\text{th}} = 1.5$. The remaining experiments we analyze consist in six independent recordings (performed on different days and with different individuals) of $N = 8$ fish during 30 min (90 000 frames), three recordings of $N = 16$ fish during 30 min, three recordings of $N = 32$ fish during 30 min, and three recordings of $N = 50$ fish during 60 min (180 000 frames). The data with $N = 8$ fish were previously used in Ref. [74].

APPENDIX B: TURNING RATE FORMULA

The turning rate ω is defined as the absolute value of the rate of change of the orientation θ of the velocity of an individual with time, i.e.,

$$\omega \equiv \left| \frac{d\theta}{dt} \right|.$$

Consider the velocity vector in two instants of time t and $t + \Delta t$. The change of orientation $\Delta \theta$ from $\vec{v}(t)$ to $\vec{v}(t + \Delta t)$ is given by

$$\sin(\Delta\theta) = \frac{\vec{v}(t) \times \vec{v}(t + \Delta t)}{v(t + \Delta t)v(t)}.$$

In the limits $\Delta t \to 0$ and $\Delta \theta \to 0$, we have

$$\sin(\Delta\theta) \simeq \frac{1}{v(t + \Delta t)v(t)} \{\vec{v}(t) \times [\vec{a}(t)\Delta t + \vec{v}(t)]\}$$

$$= \frac{\vec{v}(t) \times \vec{a}(t)}{v(t + \Delta t)v(t)} \Delta t \simeq \Delta\theta,$$

where $\vec{a}(t)$ is the fish acceleration. Then we can write

$$\frac{d\theta}{dt} = \lim_{\Delta t \to 0} \frac{\Delta\theta}{\Delta t} = \lim_{\Delta t \to 0} \frac{\vec{v}(t) \times \vec{a}(t)}{v(t + \Delta t)v(t)} = \frac{\vec{v}(t) \times \vec{a}(t)}{v(t)^2},$$

recovering the expression for the turning rate in Eq. (1).

APPENDIX C: NULL MODEL OF AVALANCHES WITHOUT TEMPORAL CORRELATIONS

Following Ref. [19], we can consider a null model of avalanche behavior in schooling fish in which individuals perform random uncorrelated turning rates, extracted from the empirical distribution $P(\omega)$. In this case, the probability q that, at a given frame, a fish performs a turning rate larger than a threshold ω_{th} (i.e., a fish is active) is given by

$$q = \int_{\omega_{\text{th}}}^{\infty} P(\omega)d\omega,$$

while the probability that, at a given frame, at least one fish in a school of N individuals performs a turning rate larger than ω_{th} (i.e., there is at least one active fish) is

$$Q = 1 - (1 - q)^N.$$

In this null model, an avalanche of duration T implies T consecutive frames with at least an active fish, followed by a frame with no active fish. Thus the duration distribution has the normalized form

$$P_0(T) = \frac{1 - Q}{Q} Q^T, \quad T \in [1, \infty). \tag{C1}$$

An interevent time t_i consists, analogously, of t_i consecutive frames with no active fish, followed by a frame with at least one active fish. Therefore, the interevent time distribution has the form

$$P_0(t_i) = \frac{Q}{1 - Q}(1 - Q)^{t_i}, \quad t_i \in [1, \infty). \tag{C2}$$

Finally, the size distribution can be estimated as follows [19]. At each frame during an avalanche, the average number of active fish is Nq/Q, where the normalization factor Q accounts for the fact that at least one fish was active in the frame considered. Thus, an avalanche of duration T has an average size $S = TNq/Q$. Transforming the duration distribution (C1), we then have [19]

$$P_0(S) = \frac{1 - Q}{Nq} Q^{QS/Nq}.$$

In all cases, we recover distributions with an exponentially decaying form.

Now the activity rate r, defined as the probability that a randomly chosen frame belongs to an avalanche, is equal to the probability that in a randomly chosen frame there is at least one active fish. This trivially implies $r = Q$, that is, the duration and interevent time distributions depend only on the activity rate and can be made to collapse for different values of N and ω_{th} leading to the same value of r. On the other hand, the size distribution depends additionally on N and q and thus cannot be made to collapse by fixing r.

For the interevent time distribution (C2), we can write, in the limit of small Q,

$$P_0(t_i) \simeq Q(1 - Q)^{t_i} = Qe^{t_i \ln(1-Q)} \simeq Qe^{-Qt_i}.$$

From Eq. (C2), $\langle t_i \rangle = \sum_{t_i=1}^{\infty} t_i P_0(t_i) = 1/Q$. Thus, we have

$$P_0(t_i) \simeq \frac{1}{\langle t_i \rangle} e^{-t_i/\langle t_i \rangle},$$

recovering the scaling relation (4) with $\Phi(x) = e^{-x}$, in the limit of large $\langle t_i \rangle$.

Interestingly, the activity rate r in this null model follows the empirical behavior shown in Fig. 1(b), as Q is a growing function of N and a decreasing function of ω_{th}.

APPENDIX D: STATISTICAL DRAGON KING DETECTION TEST

The statistical dragon king detection test developed in [49] and also employed in [48] uses a p value to quantify the presence of a dragon king peak in the tail of a heavy-tailed distributed variable x. First, the complementary cumulative distribution function $1 - F(x) \equiv P(X \geqslant x)$ is constructed and the most overrepresented data point in the tail, denoting

potential dragon king events, is identified. Next a power law ax^b is fitted to the appropriate scale-free region of $1 - F(x)$. Confidence intervals γ of the power law fit are calculated from [49]

$$\left(\frac{1}{N} q_{1-\gamma/2}(N, ax^b), \frac{1}{N} q_{\gamma/2}(N, ax^b) \right],$$

where $q_\alpha(n, z)$ is the α quantile of the binomial distribution $B(n, z)$ and N is the number of elements x. Finally, the tightest confidence interval γ^* of the power-law fit accommodating for the most overrepresented data point in the tail is obtained by visual inspection. The p value of the null hypothesis that there are no dragon kings in the distribution corresponds to $p \equiv 1 - \gamma^*$.

[1] H. E. Stanley, *Introduction to Phase Transitions and Critical Phenomena* (Oxford University Press, New York, 1987).

[2] J. J. Binney, N. J. Dowrick, A. J. Fisher, and M. E. J. Newman, *The Theory of Critical Phenomena: An Introduction to the Renormalization Group* (Oxford University Press, New York, 1992).

[3] J. M. Yeomans, *Statistical Mechanics of Phase Transitions* (Clarendon, Oxford, 1992).

[4] M. A. Muñoz, *Colloquium*: Criticality and dynamical scaling in living systems, Rev. Mod. Phys. **90**, 031001 (2018).

[5] T. Mora and W. Bialek, Are biological systems poised at criticality? J. Stat. Phys. **144**, 268 (2011).

[6] J. Beggs and N. Timme, Being critical of criticality in the brain, Front. Physiol. **3**, 163 (2012).

[7] K. Binder, Finite size scaling analysis of Ising model block distribution functions, Z. Phys. B **43**, 119 (1981).

[8] P. Romanczuk and B. C. Daniels, in *Order, Disorder and Criticality: Advanced Problems of Phase Transition Theory*, edited by Y. Holovatch (World Scientific, Singapore, 2022), Vol. 7, pp. 179–208.

[9] D. J. T. Sumpter, *Collective Animal Behavior* (Princeton University Press, Princeton, 2010).

[10] T. Vicsek and A. Zafeiris, Collective motion, Phys. Rep. **517**, 71 (2012).

[11] J. Toner and Y. Tu, Flocks, herds, and schools: A quantitative theory of flocking, Phys. Rev. E **58**, 4828 (1998).

[12] T. Vicsek, A. Czirók, E. Ben-Jacob, I. Cohen, and O. Shochet, Novel type of phase transition in a system of self-driven particles, Phys. Rev. Lett. **75**, 1226 (1995).

[13] I. D. Couzin, J. Krause, R. James, G. D. Ruxton, and N. R. Franks, Collective memory and spatial sorting in animal groups, J. Theor. Biol. **218**, 1 (2002).

[14] K. Tunstrøm, Y. Katz, C. C. Ioannou, C. Huepe, M. J. Lutz, and I. D. Couzin, Collective states, multistability and transitional behavior in schooling fish, PLoS Comput. Biol. **9**, e1002915 (2013).

[15] *Fish Cognition and Behavior*, edited by C. Brown, K. N. Laland, and J. Krause, Fish and Aquatic Resources Series No. 11 (Blackwell, Oxford, 2006).

[16] S. B. Rosenthal, C. R. Twomey, A. T. Hartnett, H. S. Wu, and I. D. Couzin, Revealing the hidden networks of interaction in mobile animal groups allows prediction of complex behavioral contagion, Proc. Natl. Acad. Sci. USA **112**, 4690 (2015).

[17] J. E. Herbert-Read, J. Buhl, F. Hu, A. J. W. Ward, and D. J. T. Sumpter, Initiation and spread of escape waves within animal groups, R. Soc. Open Sci. **2**, 140355 (2015).

[18] V. Lecheval, L. Jiang, P. Tichit, C. Sire, C. K. Hemelrijk, and G. Theraulaz, Social conformity and propagation of information in collective U-turns of fish schools, Proc. R. Soc. B **285**, 20180251 (2018).

[19] J. Múgica, J. Torrents, J. Cristín, A. Puy, M. C. Miguel, and R. Pastor-Satorras, Scale-free behavioral cascades and effective leadership in schooling fish, Sci. Rep. **12**, 10783 (2022).

[20] L. Gómez-Nava, R. T. Lange, P. P. Klamser, J. Lukas, L. Arias-Rodriguez, D. Bierbach, J. Krause, H. Sprekeler, and P. Romanczuk, Fish shoals resemble a stochastic excitable system driven by environmental perturbations, Nat. Phys. **19**, 663 (2023).

[21] G. Kastberger, E. Schmelzer, and I. Kranner, Social waves in giant honeybees repel hornets, PLoS ONE **3**, e3141 (2008).

[22] W. K. Potts, The chorus-line hypothesis of manoeuvre coordination in avian flocks, Nature (London) **309**, 344 (1984).

[23] A. Procaccini, A. Orlandi, A. Cavagna, I. Giardina, F. Zoratto, D. Santucci, F. Chiarotti, C. K. Hemelrijk, E. Alleva, G. Parisi, and C. Carere, Propagating waves in starling, *Sturnus vulgaris*, flocks under predation, Anim. Behav. **82**, 759 (2011).

[24] A. Attanasi, A. Cavagna, L. Del Castello, I. Giardina, T. S. Grigera, A. Jelić, S. Melillo, L. Parisi, O. Pohl, E. Shen, and M. Viale, Information transfer and behavioural inertia in starling flocks, Nat. Phys. **10**, 691 (2014).

[25] F. Ginelli, F. Peruani, M.-H. Pillot, H. Chaté, G. Theraulaz, and R. Bon, Intermittent collective dynamics emerge from conflicting imperatives in sheep herds, Proc. Natl. Acad. Sci. USA **112**, 12729 (2015).

[26] B. C. Daniels, D. C. Krakauer, and J. C. Flack, Control of finite critical behaviour in a small-scale social system, Nat. Commun. **8**, 14301 (2017).

[27] W. Bialek, A. Cavagna, I. Giardina, T. Mora, E. Silvestri, M. Viale, and A. M. Walczak, Statistical mechanics for natural flocks of birds, Proc. Natl. Acad. Sci. USA **109**, 4786 (2012).

[28] A. Cavagna, L. Del Castello, I. Giardina, T. Grigera, A. Jelic, S. Melillo, T. Mora, L. Parisi, E. Silvestri, M. Viale, and A. M. Walczak, Flocking and turning: A new model for self-organized collective motion, J. Stat. Phys. **158**, 601 (2015).

[29] V. Mwaffo and F. Vernerey, Analysis of group of fish response to startle reaction, J. Nonlinear Sci. **32**, 96 (2022).

[30] W. Poel, B. C. Daniels, M. M. G. Sosna, C. R. Twomey, S. P. Leblanc, I. D. Couzin, and P. Romanczuk, Subcritical escape waves in schooling fish, Sci. Adv. **8**, eabm6385 (2022).

[31] S. Bikhchandani, D. Hirshleifer, and I. Welch, A theory of fads, fashion, custom, and cultural change as informational cascades, J. Polit. Econ. **100**, 992 (1992).

[32] A. Attanasi, A. Cavagna, L. Del Castello, I. Giardina, S. Melillo, L. Parisi, O. Pohl, B. Rossaro, E. Shen, E. Silvestri, and M. Viale, Finite-size scaling as a way to probe near-criticality in natural swarms, Phys. Rev. Lett. **113**, 238102 (2014).

[33] A. Attanasi, A. Cavagna, L. D. Castello, I. Giardina, S. Melillo, L. Parisi, O. Pohl, B. Rossaro, E. Shen, E. Silvestri, and M. Viale, Collective behaviour without collective order in wild swarms of midges, PLoS Comput. Biol. **10**, e1003697 (2014).

[34] A. Cavagna, A. Cimarelli, I. Giardina, G. Parisi, R. Santagati, F. Stefanini, and M. Viale, Scale-free correlations in starling flocks, Proc. Natl. Acad. Sci. USA **107**, 11865 (2010).

[35] M. M. G. Sosna, C. R. Twomey, J. Bak-Coleman, W. Poel, B. C. Daniels, P. Romanczuk, and I. D. Couzin, Individual and collective encoding of risk in animal groups, Proc. Natl. Acad. Sci. USA **116**, 20556 (2019).

[36] G. Pruessner, *Self-Organised Criticality: Theory, Models and Characterisation* (Cambridge University Press, Cambridge, 2012).

[37] F. Salvat, in *Proceedings of the Workshop on PENELOPE-2018: A Code System for Monte Carlo Simulation of Electron and Photon Transport, Barcelona, 2019* (OECD Nuclear Energy Agency, Boulogne-Billancourt, 2019).

[38] S. Zapperi, *Crackling Noise: Statistical Physics of Avalanche Phenomena* (Oxford University Press, Oxford, 2022).

[39] See Supplemental Material at http://link.aps.org/supplemental/10.1103/PhysRevResearch.6.033270 for videos and figures.

[40] W. Zhong, Y. Deng, and D. Xiong, Burstiness and information spreading in active particle systems, Soft Matter **19**, 2962 (2023).

[41] Á. Corral, Universal local versus unified global scaling laws in the statistics of seismicity, Physica A **340**, 590 (2004).

[42] J. Baró, J.-M. Martín-Olalla, F. J. Romero, M. C. Gallardo, E. K. H. Salje, E. Vives, and A. Planes, Avalanche correlations in the martensitic transition of a Cu–Zn–Al shape memory alloy: Analysis of acoustic emission and calorimetry, J. Phys.: Condens. Matter **26**, 125401 (2014).

[43] M. C. Kuntz and J. P. Sethna, Noise in disordered systems: The power spectrum and dynamic exponents in avalanche models, Phys. Rev. B **62**, 11699 (2000).

[44] J. P. Sethna, K. A. Dahmen, and C. R. Myers, Crackling noise, Nature (London) **410**, 242 (2001).

[45] N. Friedman, S. Ito, B. A. W. Brinkman, M. Shimono, R. E. L. DeVille, K. A. Dahmen, J. M. Beggs, and T. C. Butler, Universal critical dynamics in high resolution neuronal avalanche data, Phys. Rev. Lett. **108**, 208102 (2012).

[46] D. Sornette, Dragon-kings, black swans and the prediction of crises, Int. J. Terraspace Sci. Eng. **2**, 1 (2009).

[47] D. Sornette and G. Ouillon, Dragon-kings: Mechanisms, statistical methods and empirical evidence, Eur. Phys. J. Spec. Top. **205**, 1 (2012).

[48] G. Mikaberidze, A. Plaud, and R. M. D'Souza, Dragon kings in self-organized criticality systems, Phys. Rev. Res. **5**, L042013 (2023).

[49] J. Janczura and R. Weron, Black swans or dragon-kings? A simple test for deviations from the power law, Eur. Phys. J. Spec. Top. **205**, 79 (2012).

[50] D. Weihs, Energetic advantages of burst swimming of fish, J. Theor. Biol. **48**, 215 (1974).

[51] R. Harpaz, G. Tkačik, and E. Schneidman, Discrete modes of social information processing predict individual behavior of fish in a group, Proc. Natl. Acad. Sci. USA **114**, 10149 (2017).

[52] G. Li, I. Ashraf, B. François, D. Kolomenskiy, F. Lechenault, R. Godoy-Diana, and B. Thiria, Burst-and-coast swimmers optimize gait by adapting unique intrinsic cycle, Commun. Biol. **4**, 40 (2021).

[53] J. E. Herbert-Read, E. Rosén, A. Szorkovszky, C. C. Ioannou, B. Rogell, A. Perna, I. W. Ramnarine, A. Kotrschal, N. Kolm, J.

Krause, and D. J. T. Sumpter, How predation shapes the social interaction rules of shoaling fish, Proc. R. Soc. B **284**, 20171126 (2017).

[54] D. S. Calovi, A. Litchinko, V. Lecheval, U. Lopez, A. P. Escudero, H. Chaté, C. Sire, and G. Theraulaz, Disentangling and modeling interactions in fish with burst-and-coast swimming reveal distinct alignment and attraction behaviors, PLoS Comput. Biol. **14**, e1005933 (2018).

[55] C. H. Scholz, *The Mechanics of Earthquakes and Faulting*, 3rd ed. (Cambridge University Press, Cambridge, 2019).

[56] F. Omori, On the after-shocks of earthquakes, J. College Sci. **7**, 111 (1894).

[57] B. Gutenberg and C. F. Richter, Earthquake magnitude, intensity, energy, and acceleration, Bull. Seismol. Soc. Am. **32**, 163 (1942).

[58] M. Baiesi and M. Paczuski, Scale-free networks of earthquakes and aftershocks, Phys. Rev. E **69**, 066106 (2004).

[59] M. Baiesi and M. Paczuski, Complex networks of earthquakes and aftershocks, Nonlinear Process. Geophys. **12**, 1 (2005).

[60] I. Zaliapin, A. Gabrielov, V. Keilis-Borok, and H. Wong, Clustering analysis of seismicity and aftershock identification, Phys. Rev. Lett. **101**, 018501 (2008).

[61] I. Zaliapin and Y. Ben-Zion, Earthquake declustering using the nearest-neighbor approach in space-time-magnitude domain, J. Geophys. Res.: Sol. Ea. **125**, e2018JB017120 (2020).

[62] G. Ouillon and D. Sornette, Magnitude-dependent Omori law: Theory and empirical study, J. Geophys. Res.: Sol. Ea. **110**, B04306 (2005).

[63] D. Sornette, *Critical Phenomena in Natural Sciences: Chaos, Fractals, Selforganization, and Disorder: Concepts and Tools*, 2nd ed., Springer Series in Synergetics (Springer, Berlin, 2004).

[64] B. Tadić and R. Melnik, Self-organised critical dynamics as a key to fundamental features of complexity in physical, biological, and social networks, Dynamics **1**, 181 (2021).

[65] M. M. Dankulov, R. Melnik, and B. Tadić, The dynamics of meaningful social interactions and the emergence of collective knowledge, Sci. Rep. **5**, 12197 (2015).

[66] B. Tadić, M. M. Dankulov, and R. Melnik, Mechanisms of self-organized criticality in social processes of knowledge creation, Phys. Rev. E **96**, 032307 (2017).

[67] L. Jiang, L. Giuggioli, A. Perna, R. Escobedo, V. Lecheval, C. Sire, Z. Han, and G. Theraulaz, Identifying influential neighbors in animal flocking, PLoS Comput. Biol. **13**, e1005822 (2017).

[68] V. Joshi, S. Popp, J. Werfel, and H. F. McCreery, Alignment with neighbours enables escape from dead ends in flocking models, J. R. Soc. Interface **19**, 20220356 (2022).

[69] W. Wu, W. Yi, X. Wang, E. Wang, and X. Zheng, Experimental study on the decision-making and motion behavior of subgroups when facing a static obstacle during movement, Expert Syst. Appl. **242**, 122761 (2024).

[70] A. Cavagna, I. Giardina, and F. Ginelli, Boundary information inflow enhances correlation in flocking, Phys. Rev. Lett. **110**, 168107 (2013).

[71] W. Hamilton, Geometry for the selfish herd, J. Theor. Biol. **31**, 295 (1971).

[72] E. Gimeno, V. Quera, F. S. Beltran, and R. Dolado, Differences in shoaling behavior in two species of freshwater fish (*Danio rerio* and *Hyphessobrycon herbertaxelrodi*), J. Comp. Psychol. **130**, 358 (2016).

[73] F. Romero-Ferrero, M. G. Bergomi, R. C. Hinz, F. J. H. Heras, and G. G. de Polavieja, idtracker.ai: Tracking all individuals in small or large collectives of unmarked animals, Nat. Methods **16**, 179 (2019).

[74] A. Puy, E. Gimeno, J. Torrents, P. Bartashevich, M. C. Miguel, R. Pastor-Satorras, and P. Romanczuk, Selective social interactions and speed-induced leadership in schooling fish, Proc. Natl. Acad. Sci. USA **121**, e2309733121 (2024).

[75] M. S. Nixon and A. S. Aguado, *Feature Extraction and Image Processing*, 2nd ed. (Academic, Amsterdam, 2010).

[76] P. Virtanen, R. Gommers, T. E. Oliphant, M. Haberland, T. Reddy, D. Cournapeau, E. Burovski, P. Peterson, W. Weckesser, J. Bright, S. J. van der Walt, M. Brett, J. Wilson, K. J. Millman, N. Mayorov, A. R. J. Nelson, E. Jones, R. Kern, E. Larson, C. J. Carey *et al.*, SciPy 1.0: Fundamental algorithms for scientific computing in Python, Nat. Methods **17**, 261 (2020).